

Water entry dynamics of spheres with heterogeneous wetting properties

Daren A. Watson ¹, Joshua M. Bom ², Madison P. Weinberg ², Christopher J. Souchik,²
and Andrew K. Dickerson ^{2,*}

¹*Department of Mechanical Engineering, Florida Polytechnic University, Lakeland, Florida 33805, USA*

²*Department of Mechanical and Aerospace Engineering, University of Central Florida,
Orlando, Florida 32816, USA*



(Received 16 April 2020; accepted 1 April 2021; published 21 April 2021)

Water entry studies traditionally employ homogeneous projectiles of varying impactor shape, entry speed, and surface roughness. Surface heterogeneity is yet another means to manipulate splash dynamics. In this experimental study, we systematically investigate the water entry of smooth, free-falling, hemispherically coated spheres for Froude numbers in the range of 2.8 – 6.7. Hydrophilic spheres are hemispherically coated with a hydrophobic compound and in-turn produce deep seal cavities, provoke changes in super-surface splash features, and alter sphere trajectories. Generally, flow separation is initialized when hydrophobic surfaces make contact with the fluid, leading to air-entrainment across the range of entry speeds and impact orientations on test. Cavity formation induced by the hydrophobic portion of a hemispherically coated sphere promotes flow separation across the hydrophilic surface at impact velocities well below the threshold of 8 m/s required for air-entrainment by completely hydrophilic spheres. Spheres having partially hydrophilic and partially hydrophobic surfaces entering the fluid simultaneously, experience asymmetric cavities and horizontal forces that result in lateral migration from straight-line trajectories. Such observations augur well for water entry applications where the coupled dynamics of flow separation and passive trajectory control are desirable.

DOI: [10.1103/PhysRevFluids.6.044003](https://doi.org/10.1103/PhysRevFluids.6.044003)

I. INTRODUCTION

Water entry of spherical impactors have been studied extensively since the seminal work of Worthington [1–10] in the late 19th century, and is relevant to applications in animal locomotion [11–13], missile water entry [14–23], aquatic sports [24,25], sea-surface landing [26,27], toilet dynamics [28–31], and underwater transport [28–30]. The vast majority of water entry studies have been performed with impactors having homogeneous wetting properties. The water entry of purely hydrophilic spheres into a liquid bath generates minimal fluid displacement and no air-entrainment [32] (Movie S1), at entry speeds [5] below $U \approx 8$ m/s. Upon impact, a thin film of liquid travels radially upwards along the sphere's periphery, converging at the apex to form an axisymmetric Worthington jet [10,28] inversely proportional to the fluid's surface tension and viscosity at low Bond numbers [33–37]. Conversely, flow separation arising from the water entry of cavity-producing impactors yield more pronounced radial splash crowns [38], and significantly higher Worthington jets [28–30] compared to their hydrophilic counterparts [32] (Movie S2). Flow separation may be instigated by purely hydrophilic impactors without altering surface roughness or entry speeds. The water entry of spinning spheres [18]; placement of tiny droplets near the equator of free-falling hydrophilic spheres [39]; sphere impacts onto buoyant, nonwoven fabric sheets placed

*Corresponding author: dickerson@ucf.edu

atop the free surface [28–30]; and the water entry of heated spheres [25] at temperatures above the Leidenfrost temperature, all achieve flow separation at speeds [5] well below 8 m/s.

Recent studies show directional control of autonomous objects is possible without active propulsion, which warrants deeper investigation into impactors with heterogeneous wetting properties [24,40,41]. Few studies from the compendium of fluid engineering research have considered such impactors. One such study investigated the path of slender axisymmetric projectiles with heterogeneous surface treatments and elucidated the influence of the leading edge geometry and impact angle on impactor trajectory [40]. At impact velocities below 8 m/s, surface roughness destabilizes the three-phase contact line along hydrophilic surfaces to alter flow separation [24]. In contrast, the impact angle of partially coated cylinders has a greater influence on their trajectories than surface roughness when inertial effects dominate water entry [24]. Tuning flow separation by way of surface treatment can also promote localized air-entrainment as observed during the water entry of stripe-coated hydrophilic cylinders [42], and hemispherically coated spheres [18,19]. These previous studies have not yet established the response of splash features to surface heterogeneity, given their focus primarily on impactor drag.

In this experimental study, we provide a systematic investigation of cavity depths, supersurface splash features, and sphere migration from the straight-line axis of entry with respect to surface heterogeneity, in the range of Froude number $Fr = U/\sqrt{gD} = 2.8 - 6.7$, where $U = \sqrt{2gh}$ is the impact velocity, $h = 10 - 50$ cm is the sphere drop heights, $g = 9.81$ m/s² is the acceleration due to gravity, and D is the sphere diameter. Thus, we show splash dynamics during fluid entry are tunable by altering wetting properties along fractional portions of the impactor surface. Half-cavities are produced when both the hydrophilic, and hydrophobic surfaces make contact with the fluid simultaneously [18,19]. As half-hydrophobic, half-hydrophilic spheres descend at the relatively low impact velocities in our tests ($U \leq 3.13$ m/s), fluid separates downstream of the stagnation point along the hydrophilic surface while separating nearer the stagnation point for the hydrophobic surface, as shown in Fig. S1. Air-entrainment is thus biased toward the hydrophobic portion of hemispherically coated spheres, effectively forming half-cavities. The pressure distribution [43] arising from this uneven cavity formation results in the lateral migration of a sphere from its straight-line trajectory [18,19]. Numerical investigations of cavities generated by half-hydrophilic, half-hydrophobic spheres based on solving the Navier-Stokes equations, coupled with the volume of fluid and continuum surface force methods, predict experimental results showing the formation of asymmetric cavities and cardioid splashes, resulting in the lateral migration of spheres [8]. We present our experimental methods for impactor surface treatment, splash visualization, and geometric measurements in Sec. II. Results are presented in Sec. III and the implications of this work discussed in Sec. IV. We provide the conclusions of our work in Sec. V.

II. METHODS

A. Impactor surface treatment

Delrin spheres with density $\rho_s = 1340$ kg/m³, masses $m = 4.9, 7.7,$ and 11.5 g and diameters $D = 1.9, 2.2,$ and 2.5 cm are cleaned in their entirety with 99% isopropyl alcohol and allowed to dry in a closed container. The surface of the spheres that are to remain hydrophilic are masked with tape and rested in circular cutouts on an acrylic sheet which holds spheres in place. The portion of the spheres left exposed atop the acrylic sheet are sprayed with Rustoleum NeverWet. We henceforth refer to these hemispherically coated spheres as $\alpha = 0.33$ and $\alpha = 0.50$, as depicted in Fig. 1(a). The coated portion of the sphere may be described as if the sphere had been submerged in the hydrophobic compound to $1/3$ or $1/2$ its diameter, respectively. With the spray nozzle $15 - 30$ cm from the exposed surfaces, spheres are sprayed twice with the Base Coat and allowed to dry for 30 min, before twice applying the Top Coat [29]. Coated impactors are allowed to cure for at least 12 h before use in experiments. Just prior to each impact trial, we again clean the hydrophilic surface with 99% isopropyl alcohol. The equilibrium and advancing contact angles of coated surfaces

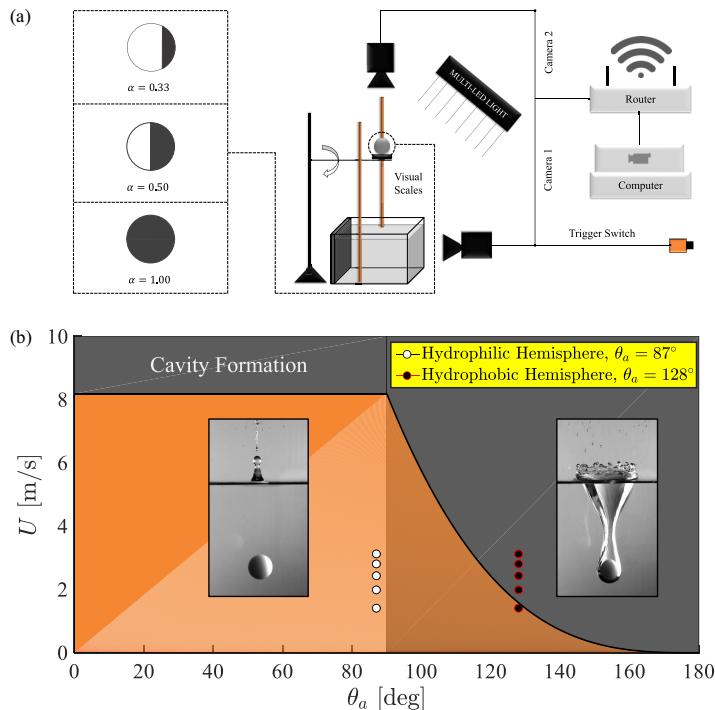


FIG. 1. (a) Schematic of experimental setup. High-speed cameras capture frontal (Photron Mini AX–100) and overhead (Photron Mini UX–100) views with diffuse lighting positioned behind the glass tank and above the frontal camera. Optional trigger switch complements manual controls in video recording software on computer. Wireless router enables multicamera synchronization. (b) Threshold velocity U for cavity formation as a function of the advancing contact angle θ_a . Solid lines are theoretical predictions based on the seminal work of Duez *et al.* [5]. We note that sphere and cavity reflections are visible along the back wall of the aquarium due to illumination from the light source positioned above the frontal camera.

are $\theta_e = 105^\circ \pm 2^\circ$ and $\theta_a = 128^\circ \pm 4^\circ$ ($N = 6$), respectively, measured photographically [28–30] using a syringe to deposit water onto the sphere’s surface. In contrast, the equilibrium and advancing contact angles on the uncoated surfaces are $\theta_e = 75^\circ \pm 4^\circ$ and $\theta_a = 87^\circ \pm 3^\circ$ ($N = 6$), respectively. These advancing contact angles, and the interaction of fluid with spheres of similar wetting properties are shown in Fig. 1(b), according to the predictions of Duez *et al.* (2007) [5]. A line of demarcation is drawn circumferentially with a fine-tip permanent marker to visually separate hydrophilic and hydrophobic zones on the spheres. The marker ink does not substantially influence the wetting properties of an untreated surface. After no more than 15 impact trials, a sphere is cleaned by a soak in 100% acetone for 1 min, followed by the aforementioned cleaning with 99% isopropyl alcohol. This treatment removes the NeverWet Coating so that spheres may be recoated.

B. Impact experiments

Spheres are released from drop heights $h = 10\text{--}50$ cm into a 65-L, 36-cm deep tempered-glass aquarium, filled halfway with tap water as shown in Fig. 1(a). The drop apparatus and experimental protocols used for impact trials are detailed in our previous works [28–30]. For splash visualization and tracking, we film water entry with a Photron Mini AX–100 high-speed camera at 1000 frames per second with resolution of 1028×1028 pixels using a 120-mm Nikon lens. Our chosen field of view is 21.5×21.5 cm², yielding a 47.8 pixel/cm magnification. Geometric measurements such as

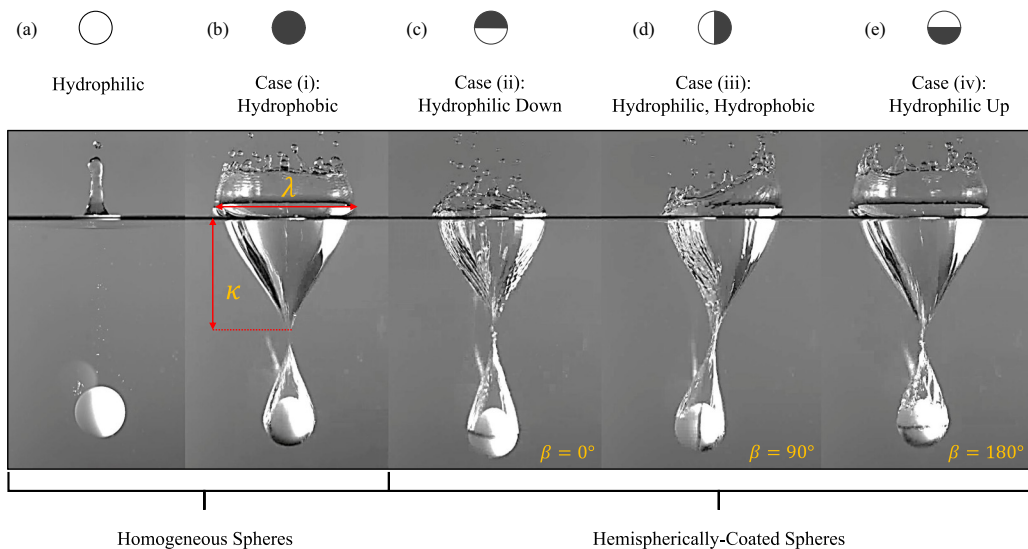


FIG. 2. Cavity formation and splash crown ascension for the water entry of a (a) fully hydrophilic sphere, (b) fully hydrophobic sphere, (c) heterogeneous sphere, $\alpha = 0.50$, $\beta = 0^\circ$; (d) heterogeneous sphere, $\alpha = 0.50$, $\beta = 90^\circ$; and (e) heterogeneous sphere, $\alpha = 0.50$, $\beta = 180^\circ$. Grey-shaded semicircle indicates hydrophobic region and white-shaded area indicates hydrophilic region. Here, κ is the depth of the cavity at the moment of cavity pinch-off, and λ is the width of the cavity opening at the free surface, also at the moment of cavity pinch-off. Spheres pictured have diameter $D = 2.5$ cm and $Fr = 4.9$. We note that sphere and cavity reflections are visible along the back wall of the aquarium due to illumination from the light source positioned above the frontal camera.

cavity depths κ and widths λ are extracted from captured videos using TRACKER, an open source image analysis software [29].

III. RESULTS

The water entry of cavity-producing projectiles can be summarized in stages, namely: collision with the free surface; air-entrainment; splash crown ascension; cavity closure and collapse; and Worthington jet projection. In this study, water entry stages are influenced by the coating configuration and release orientation of spheres on test. We impact the quiescent, unbounded free surface of a deep aqueous pool with hemispherically coated spheres from various drop heights in the range $h = 10 - 50$ cm. Four cavity-producing entry cases are considered: (i) fully hydrophobic sphere ($\alpha = 1.00$); (ii) heterogeneous sphere, impacting the free surface along the hydrophilic hemisphere, $\beta = 0^\circ$; (iii) heterogeneous sphere, impacting the free surface along the line of demarcation, $\beta = 90^\circ$, and (iv) heterogeneous sphere, impacting the free surface along the hydrophobic hemisphere, $\beta = 180^\circ$. These four impact cases are graphically depicted in Fig. 2. Flow separation is achieved for all water entry permutations (i)–(iv), on test, which stands in contrast to their purely hydrophilic counterparts. We discuss these in turn.

A. Impactor surface treatments modulate splash features

Above the free surface, splash crowns are influenced by impact orientation β as shown in Fig. 2. When $\beta = 0^\circ$ a radial splash crown ascends vertically upward and an axisymmetric Worthington jet propagates along the axis of fluid entry. For $0^\circ < \beta < 180^\circ$ we note a lopsided crown, where amplification of the crown corresponds to the hydrophobic portion. We rationalize this observation by noting previous studies find that splash crowns from homogeneous hydrophobic impactors are

higher than their hydrophilic counterparts [38,44,45]. Nonuniformity experienced during splash crown ascension indicates nonaxisymmetric fluid displacement. Thus, we pictorially compare cavity formation for the aforementioned water entry cases:

Case (i): Fully hydrophobic spheres impacting the liquid bath entrain air to form deep seal cavities [21] characterized by smooth cavity walls as shown in Movie S2.

Case (ii): A typical splash generated by orientation (ii), $\alpha = 0.50$ and $\beta = 0^\circ$, is shown in Movie S3. Cavities are visually distinguishable from $\alpha = 1.00$ by the jaggedness of cavity walls. In this case, flow separation is delayed until the fluid makes contact with the upward-facing hydrophobic surface of the sphere. Hence, the three-phase contact line [24] coincides with the line of demarcation. For impacts below $Fr \approx 4.9$, pinch-off occurs on average, at depths shallower than the sphere diameter D and trailing cavities [25] remain attached to descending spheres until impact with the container floor. Spheres coated hydrophobic $\alpha = 0.33$ entering the fluid with hydrophobic surface upward-facing produce surface seals for impacts below $Fr \approx 5.7$, and deep seals above. Pinch-off depth is discussed in Sec. III C.

Case (iii): Rotating impact orientation of spheres $\beta = 90^\circ$ clockwise such that the line of demarcation is perpendicular to the free surface generates asymmetric deep seal cavities and curved subsurface sphere trajectories [32], as shown in Fig. 3(a) and Movie S4. Spheres migrate from straight-line entry due to the generation of horizontal hydrodynamic forces acting perpendicular to gravity. The displacement produced by this uneven cavity formation is greater for impacts below $Fr \approx 4.0$. The role of the horizontal hydrodynamic force experienced by spheres is further discussed in Sec. III D. As spheres descend, air-entrainment is concentrated along hydrophobic hemispheres [20], shifting spheres laterally by more than a diameter for impacts below $Fr \approx 4.0$ [Fig. 3(b)]. An example of this extensive lateral shift at relatively low impact velocity is shown in Movie S5 of the Supplemental Material. The temporal evolution of an $\alpha = 0.50$, $\beta = 90^\circ$ sphere experiencing lateral translation is also displayed in Fig. 3(a). After pinch-off, cavity lift forces diminish. Smooth cavity walls develop on the hydrophobic portions of descending spheres whereas cavity walls with surface waves emanate from hydrophilic hemispheres prior to cavity collapse. The curvature of sphere trajectories during air-entrainment reduces deep seal cavity depths κ relative to homogeneous cavity-producing impactors traveling along the straight-line axis. For increasing Fr , inertial effects dominate hydrodynamic forces imposed by an anisotropic pressure distribution with spheres maintaining a nearly vertical descent as seen in Fig. 3(b).

Case (iv): Spheres with $\alpha = 0.50$, $\beta = 180^\circ$ (Movie S6) yield qualitatively similar results as homogeneous hydrophobic spheres. However, unlike homogeneous spheres, trailing cavities are not as smooth post-pinch-off [Fig. 2(e)].

B. Spatiotemporal evolution of splash features

Flow visualization typically involves still image sequences showing the temporal evolution of splash features. To better differentiate water entry dynamics of hemispherically-coated spheres, vertical slices of video frames 3 pixels in width passing through the sphere's centerline are placed adjacent to each other with time increasing from left to right as pictured in Fig. 4(a)–4(d). These spatiotemporal diagrams, also known as kymographs [46], display the water entry process in its entirety. The kymograph of a purely hydrophilic sphere pictured in Fig. 4(a) shows the rise of an ascending film above surface, and no spatiotemporal disturbance of fluid below surface, except for air bubble formation subsequent to the collapse of the Worthington jet at $t \geq 200$ ms. In contrast, cavity-producing cases are characterized by an initially rounded protuberance showing the ascension of the splash crown, followed by a more voluminous protuberance representing Worthington jets that persist beyond $t \approx 100$ ms as shown in Fig. 4(b)–4(d). Worthington jets are also amplified for heterogeneous spheres with downward-facing hydrophilic surfaces [Fig. 4(c)] due to the onset of cavity formation at the line of demarcation. Thus, bubble formation is more pronounced when compared to their hydrophilic counterparts [Fig. 4(a)] given the increased number of impacting droplets resulting from the Rayleigh-Plateau instability [47] of the Worthington jet. We note that

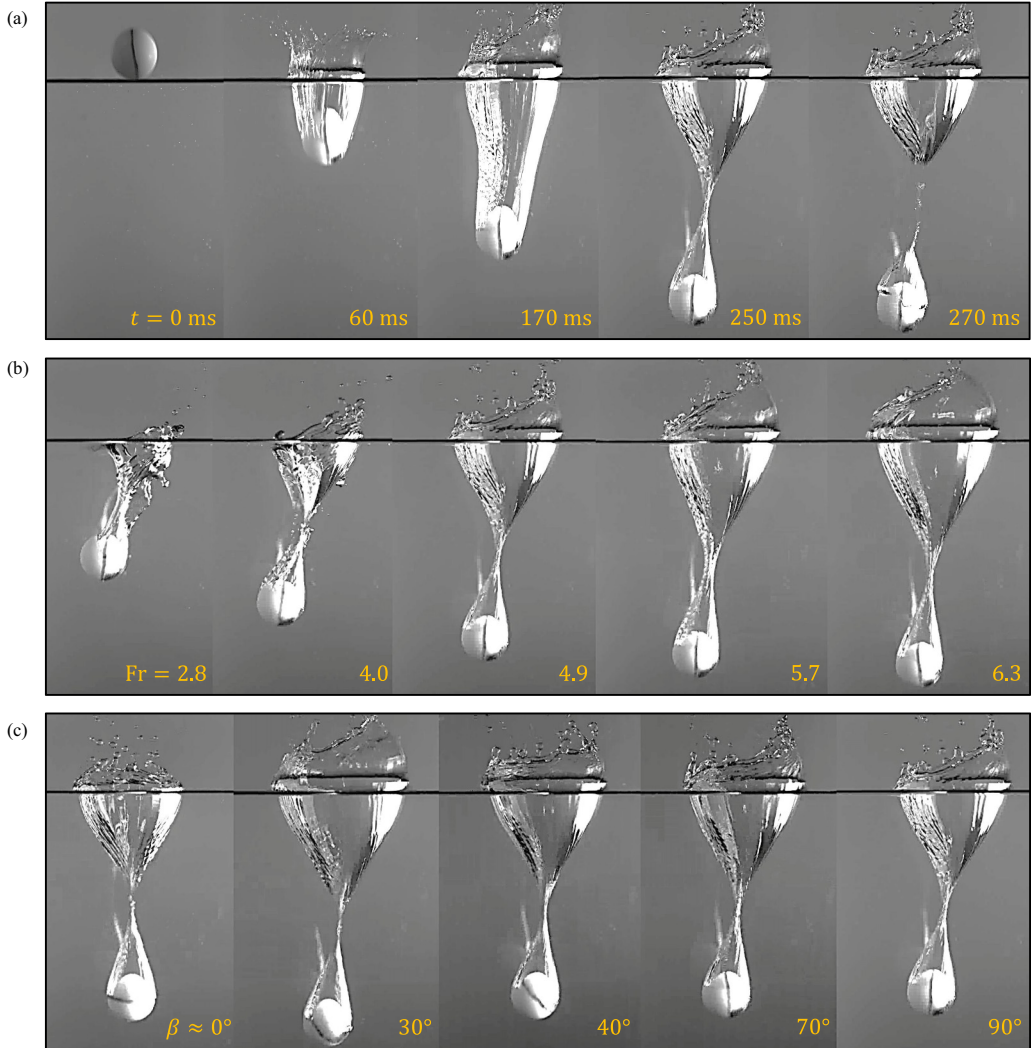


FIG. 3. (a) Temporal evolution of an air-entraining cavity and ascending splash crown for the water entry of a heterogeneous sphere, $\alpha = 0.50$, $\beta = 90^\circ$. A smooth cavity wall develops on the hydrophobic side of sphere, whereas a rough cavity wall envelops the sphere along the hydrophilic hemisphere prior to cavity pinch-off. Cavity formation and splash crown ascension for the water entry of a half-coated hydrophilic sphere making impact across the range of (b) Froude numbers Fr and, (c) impact orientations β on test. Spheres have diameter $D = 2.5$ cm. We choose $Fr = 4.9$ when iterating impact angles in (c). We note that the line of demarcation for $\beta \approx 30^\circ$ in (c) is perpendicular to the image plane despite its obscurity due to the overillumination of the right-hand side of the sphere.

the onset of jet breakup is determined by the onset of bubble formation below surface as annotated in the cavity-producing kymographs. For $\alpha = 0.50$, $\beta = 180^\circ$ [Fig. 4(d)], spatiotemporal fluid displacement is qualitatively similar to $\alpha = 1.00$ [Fig. 4(b)] with splash crowns ascending for a duration of $t \approx 100$ ms, and Worthington jets persisting up to $t \approx 500$ ms for both cases. Across all impact scenarios on display, wider sphere traces imply a slowing of the sphere during subsurface descent.

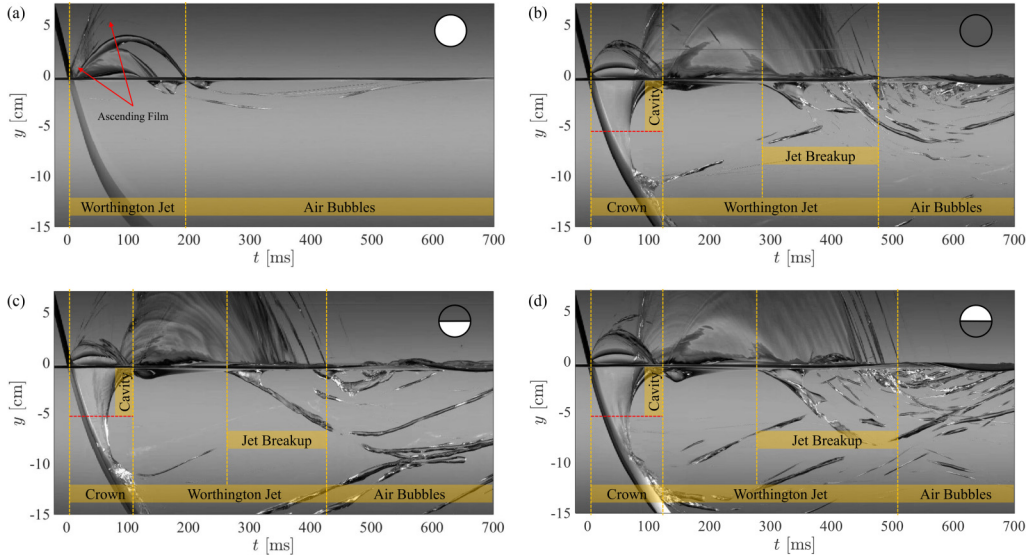


FIG. 4. Spatiotemporal diagrams showing water entry dynamics of a (a) fully hydrophilic sphere, (b) fully hydrophobic sphere, (c) heterogeneous sphere, $\alpha = 0.50$, $\beta = 0^\circ$; and (d) heterogeneous sphere, $\alpha = 0.50$, $\beta = 180^\circ$. The water entry dynamics of a heterogeneous sphere, $\alpha = 0.50$, $\beta = 90^\circ$ is shown in Fig. 6(d). Spheres pictured have diameter $D = 2.2$ cm and $Fr = 5.2$.

C. Coating scheme and impact orientation determine cavity depths

Hemispherically coated spheres striking a water bath produce air-entraining cavities for all velocities on test at any impact orientation. Hydrophobic surfaces facing the free surface ($\beta = 180^\circ$) produce cavities as if the sphere is wholly hydrophobic because separation begins well below the equator [21]. For coating permutations $\alpha = 0.33, 0.50$, cavity depths are nearly identical to those of $\alpha = 1.00$, as seen by the nearly overlapping data points of Fig. 5. Hydrophilic surfaces facing the free surface ($\beta = 0^\circ$), allow the liquid to remain attached to the sphere until passing the line of demarcation, at which point the abrupt change in wetting properties triggers separation at velocities well below the hydrophilic sphere threshold reported by Duez *et al.* [5]. A sphere coated

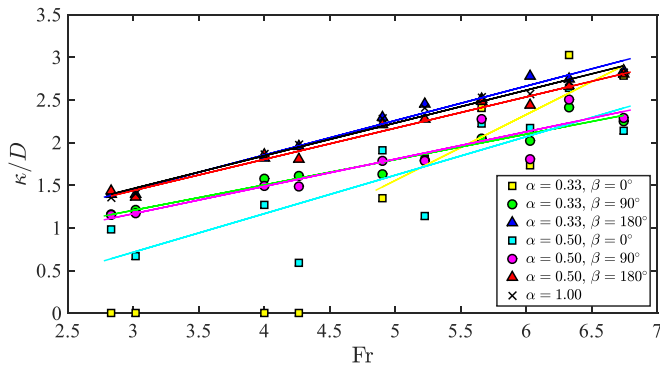


FIG. 5. Nondimensionalized cavity depths κ/D versus Fr . Disaggregated plots of nondimensionalized cavity depths κ/D versus Fr are included in Fig.S2. Deep seal cavity depths arising from the water entry of heterogenous spheres between our range of impact velocities may be described by $\kappa/D = \psi Fr + \gamma$. Best fit correlation values obtained are in the range $R^2 = 0.66 - 0.98$, with individual values given in Table I.

TABLE I. Statistical analysis of measured non-dimensionalized cavity depths κ/D and curve fitting correlation values.

Coating, α	Orientation, β	Mean κ/D	Std. Dev.	Best Fit ψ	Best Fit γ	Best Fit R^2
0.33	0°	1.12	0.20	0.77	-2.30	0.66
	90°	1.77	0.11	0.30	0.32	0.94
	180°	2.22	0.08	0.40	0.24	0.98
0.50	0°	1.57	0.26	0.45	-0.64	0.70
	90°	1.77	0.08	0.32	0.21	0.86
	180°	2.13	0.07	0.37	0.34	0.98
1.00	—	2.19	0.06	0.38	0.31	0.98

$\alpha = 0.33$ experiences flow separation at a later time than one coated $\alpha = 0.50$, producing a narrower cavity that pinches-off at a relatively shallower depth. If the line of demarcation aligns with gravity ($\beta = 90^\circ$), the hydrophobic portion induces flow separation near the south-pole, while the flow remains attached on the hydrophilic portion before eventually separating above the equator. The resulting asymmetric cavities for $\alpha = 0.33, 0.50$, are comparable, as seen in Fig. 5. The presence of the cavity produced by the hydrophobic surface triggers cavity migration to the hydrophilic side well below the critical cavity-producing velocity [5], approximately 8 m/s.

The influence of surface treatment on cavity depths can be mathematically characterized by first considering the pinch-off of the conical deep seal cavity [28] produced behind descending spheres. Recall, κ is the depth of the cavity at the moment of pinch-off. We expect *a priori*, a scaling of cavity depth at pinch-off κ to obey $\kappa/D \sim f(\text{Fr})$ for a fixed coating and orientation scheme by considering non-dimensionalized deep seal pinch-off time $t_p U/D \sim \text{Fr}$, as derived in Aristoff *et al.* [16]. Here $t_p \sim \kappa/U$ is the pinch-off time [16,18,21], which is roughly constant for cavity-producing impacts irrespective of the magnitude of sphere deceleration. As such $\kappa/D \sim \text{Fr}$. Measurements in Fig. 5, however, suggest that $\kappa/D \rightarrow 0$ before $\text{Fr} \rightarrow 0$, which is expected [5]. Thus, $\kappa/D \sim \text{Fr}$ is valid only for Froude numbers which produce cavities and an intercept γ is needed for application of the scaling relation. Accordingly, deep seal cavities produced by the water entry of heterogeneous spheres may be suitably described by

$$\kappa/D = \psi \text{Fr} + \gamma, \quad (1)$$

applied only to the nonzero portion of measurements, where ψ and γ are best fit coefficients. We plot best fits of nondimensionalized cavity depths κ/D against Fr for all impact scenarios in Fig. 5. Best fit coefficients and correlation values $R^2 = 0.66 - 0.98$ are given in Table I. For all cases in Table I, we observe a positive correlation between cavity depths κ/D and Fr . The slope for $\alpha = 0.33, \beta = 0^\circ$ is $\psi = 0.77$, which likely is a result of unstable cavity production ($R^2 = 0.66$) and does not faithfully represent broad physical behavior. In general, spheres oriented at $\beta = 0^\circ$ show large variability in non-dimensionalized cavity pinch-off depth κ/D , a likely consequence of cavity walls rife with capillary waves, like those shown in Fig. 2(c). The emergence of capillary waves on the walls is seen for separation that does not occur near the south-pole, as it does for $\alpha = 1$ [Fig. 2(b)] and all spheres oriented at $\beta = 180^\circ$ [Fig. 2(e)]. Separation at the line of demarcation is not perfectly axisymmetric due to slight deviations in impact angle and imperfections in the coating transition.

Negative γ values for $\beta = 0^\circ$ spheres demonstrate that spheres leading with hydrophilic surfaces cease cavity production prior to the other orientations tested, as velocity is decreased. Furthermore, $\alpha = 0.33, \beta = 0^\circ$ spheres are unable to produce deep seals below $\text{Fr} \approx 4.8$, and as a result, their cavity production is comparable to spheres with $\theta_a \approx 120^\circ$. For the same Fr , spheres with $\beta = 180^\circ$ produce deeper cavities than those with $\beta = 0^\circ$.

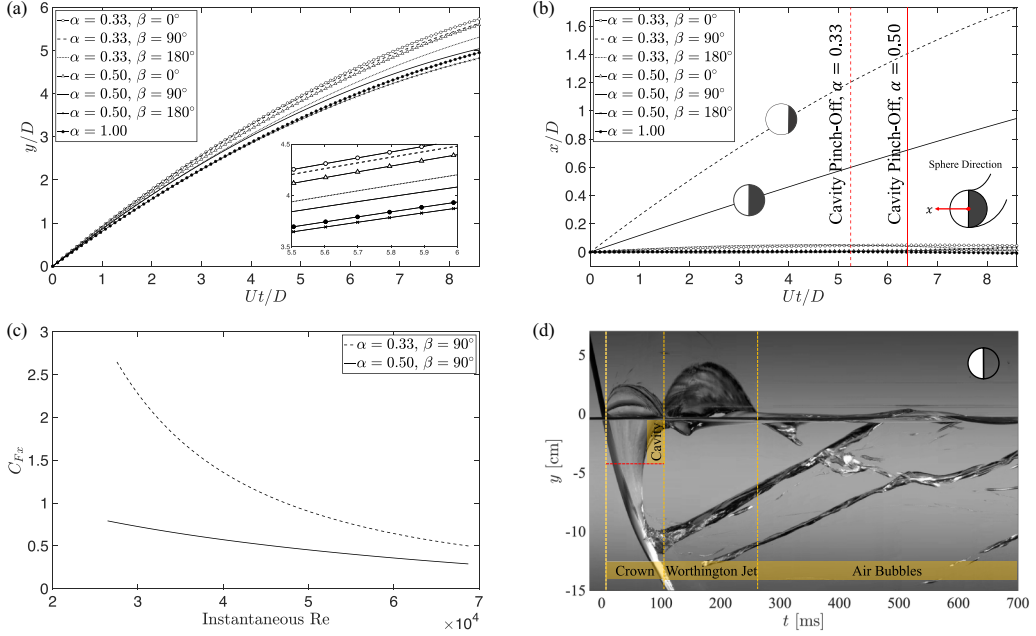


FIG. 6. Nondimensionalized (a) vertical y/D and (b) horizontal x/D positions versus dimensionless time Ut/D . The point at which the sphere's center of mass makes contact with the free surface is chosen as $y = x = 0$. Vertical lines in (b) indicate the dimensionless time Ut/D at which cavity pinch-off occurs. (c) The relation between horizontal hydrodynamics force coefficients C_{Fx} , and instantaneous Reynolds number Re . (d) Spatiotemporal diagrams showing water entry dynamics of a heterogeneous sphere, $\alpha = 0.50$, $\beta = 90^\circ$. Spheres have an impact velocity of $U = 2.4$ m/s.

D. Lateral displacement by submerged impactors, $\beta = 90^\circ$

To compare hydrodynamic forces induced by surface heterogeneity, we fix $h = 30$ cm such that $U \approx 2.4$ m/s, ($Fr = 4.9$) and track the center of mass of 2.5-cm spheres as seen in Fig. 6(a) and 6(b). Tracking begins when the center of mass of spheres passes the free surface ($x = y = 0$) and is terminated just before impact with the floor of the liquid bath. Spheres with line of demarcation perpendicular to the free surface $\beta = 90^\circ$ deviate from straight-line trajectories. While we do not explicitly quantify hydrodynamic drag in the y direction, we can infer relative levels of drag for the various coating schemes and orientations on test by considering the arrangement of curves in Fig. 6(a). It is well-known that hydrophobic spheres fall faster through a fluid than their hydrophilic counterparts due to mitigation of vortex shedding [20]. In our experiments, $\alpha = 0.33$ and $\beta = 0^\circ$ descends most rapidly, likely due to prevention of vortex shedding by cavity formation, but this sphere also permits the flow to remain attached over the majority of the surface. Such flow attachment reduces cavity width, and thus, fluid displacement. Spheres with $\beta = 180^\circ$ descend more slowly because flow separation is induced below the equator and produces a wider cavity, as pictured in Fig. 2(b) and 2(c).

As noted above, spheres with $\beta = 180^\circ$ exhibit curved subsurface trajectories. The hydrodynamic force coefficient C_{Fx} in the x direction for such spheres is given by [19]

$$C_{Fx}(t) = \frac{8(m + m_a)\ddot{x}(t)}{\rho\pi D^2 u(t)^2}, \quad (2)$$

where $\ddot{x}(t)$ is the second derivative with respect to time for the x position track, $m_a = \pi\rho D^3 C_m/6$ is the added mass which accounts for the effect of accelerating fluid by the descending sphere [28,30],

$C_m = 0.50$ is the added mass coefficient, treated as a constant value across all impact scenarios, and $u(t) = \sqrt{\dot{x}(t)^2 + \dot{y}(t)^2}$ is the instantaneous magnitude of the sphere velocity [19]. While the value of C_m likely changes as the separation line migrates throughout impact, and changes as the cavity pinches off, we choose $C_m = 0.50$ given previous work on cavity-producing impactors traversing an unbounded fluid [14–16, 18, 19, 28, 30]. As such, the absolute values of C_{Fx} must be interpreted in the context of the assumed value of $C_m = 0.50$.

To evaluate the derivatives of instantaneous experimental data, we employ numerical differentiation, and smoothing techniques provided by Watson *et al.* [30]. Our technique ensures that results of numerical differentiation do not produce explicitly nonphysical results such as negative velocity. In the context of this study, lateral x displacement measurements are first smoothed with a Savitzky-Golay filter [48] to reduce the influence of experimental error prior to numerical differentiation to obtain temporal velocity \dot{x} , and then smoothed once more prior to the final differentiation to obtain temporal acceleration \ddot{x} .

Solving Eq. (2) yields horizontal hydrodynamic force coefficients C_{Fx} for heterogeneous spheres, $\beta = 90^\circ$ in the range of instantaneous Reynolds number $Re = \rho Du(t)/\mu = 26\,000 - 69\,000$, where $\rho = 999\text{ kg/m}^3$ and $\mu = 8.90 \times 10^{-4}\text{ Pas}$ are the density and dynamic viscosity of water, respectively, as plotted in Fig. 6(c). The sphere with $\alpha = 0.33$ experiences the greatest migration with mean $C_{Fx} \approx 1.17$ when compared to $\alpha = 0.50$ with mean $C_{Fx} \approx 0.50$, as shown in Fig. 6(c). We plot y/D versus x/D for both spheres in Fig. S3. Impactors with lesser coating allow the hydrophilic side's flow to remain attached over a greater portion of the sphere surface and thus promote increased fluid momentum in the negative x direction, producing greater sphere momentum in the positive x direction as annotated in Fig. 6(b). We analyze the curved sphere trajectory spatiotemporally by creating a kymograph in which the selected pixels follow the sphere's center of mass, shown in Fig. 6(d). Super-surface splash features appear muted compared to all other cavity-producing cases shown in Fig. 4, while entrained bubbles appear fewer in number but larger in volume.

IV. DISCUSSION

This study shows that heterogeneous spheres impacting a quiescent unbounded liquid pool produce impactor surface-dependent splash features, and orientation-dependent trajectories. These results may be extended to engineering applications where the coupled dynamics of flow separation and passive trajectory control are desirable. Biologically, terrestrial and airborne organisms entering the water such as the water boatman [49–51], the common frog [52–54], and the American anhinga [55–57], may benefit from flow separation through surface heterogeneity, thus modulating their underwater acrobatics. Industrially, marine vessels may make use of surface treatments to tune flow separation for economy or performance.

On-board measurement of impact acceleration for various coating schemes is an area of future work, which we expect to reveal that the impulse at liquid contact, not discernible through image analysis, will increase as the flow front encounters the line of demarcation, and is thus highest for leading hydrophobic surfaces. Impulse is likely lowest when hydrophilic surfaces first make free surface contact because the flow remains attached over greater portions of the surface. However, the eventual creation of a cavity is instrumental in the overall minimization hydrodynamic force [20]. Such a reduction, however, is not limited to large patches of surface coating. Speirs *et al.* [58] prewetted hydrophilic spheres with a drop of water to trigger cavity formation, thus showing air entrainment is possible with coatings a fraction the size of ours. To probe this hypothesis, we coat 5% of the surface area of a 2.2-cm sphere hydrophobic ($\beta = 90^\circ$), and observe localized cavity formation and sphere migration at $Fr = 4.3$ as shown in Movie S7. As such, the extent to which very small, coated areas can produce lateral motion is a topic for further work.

The lateral migration of spheres is not only achievable through impactor surface treatment, but also through the treatment of the free surface with a compliant medium [28, 30]. Eccentric impacts onto thin, nonwoven fabrics produce similar outcomes to the those previously identified in this study. We qualitatively examine cavity evolution for a hydrophilic sphere impacting the edge of a

fabric sheet at Froude number $Fr = 2.8$, as shown in Fig. S4, and Movie S8 of the Supplemental Material [32]. The efficacy of asymmetric cavity formation by established cavity-forming techniques warrants further comparison and investigation.

Flow separates axisymmetrically from hemispherically coated spheres when the line of demarcation is parallel ($\beta = 0^\circ, 180^\circ$) to the free surface. Thus, spheres experience negligible angular rotation ω during entry. In contrast, for $\beta = 90^\circ$, uneven cavity formation and the generation of lift forces contribute to the angular rotation $\omega = 4.71 \text{ rad/s} \pm 1.89 \text{ rad/s}$ ($N = 7, Fr = 4.3$) of spheres within the first 30 ms of water entry. We note sphere rotation is insufficient for a full revolution. In the context of the work of Techet and Truscott [19], who explored the water entry of spinning spheres, we also expect sphere rotation to decrease as the impact velocity approaches a critical level for cavity formation around the entire sphere.

V. CONCLUSION

Hydrophilic spheres made heterogeneous by selectively coating parts of the surface hydrophobic produce air-entraining cavities with textures and metrics dependent on the area of surface treatment and impact orientation. Spheres with downward-facing hydrophilic surfaces experience flow separation at the line of demarcation at which the hydrophobic coating begins, surface waves on cavity walls, and trailing cavities. On the contrary, with downward-facing hydrophobic hemispheres, flow separates well below the equator while producing smooth cavity walls and trailing cavities. Generally, increases in the coated-diameter and spheres hydrophobic-down promote wider and deeper cavities. Water entry with a vertical demarcation line skews supersurface splash features, and produces sphere migration from a straight-line trajectory, where a reduction in the coated-diameter yields greater lateral displacement. Splash features and impactor motion may thus be tuned by surface heterogeneity.

ACKNOWLEDGMENTS

We acknowledge the National Science Foundation (Grant No. CBET-1941341) for financial support, and T. Truscott and R. Rabbi at the Utah State University for valuable insight. We thank J. Stephen, J. Galvez, and M. Artman-Breitung for experimental support.

-
- [1] A. M. Worthington and R. S. Cole, Impact with a liquid surface studied by the aid of instantaneous photography, *Philos. Trans. R. Soc. London, Ser. A, Containing Papers Math. Phys. Charact.* **189**, 137 (1897).
 - [2] A. M. Worthington and R. S. Cole, Impact with a liquid surface, studied by the aid of instantaneous photography Paper II, *Proc. R. Soc. Lond* **65**, 153 (1900).
 - [3] A. M. Worthington, *A Study of Splashes* (Longmans, Green and Co., London, 1908).
 - [4] S. T. Thoroddsen, T. G. Etoh, K. Takehara, and Y. Takano, Impact jetting by a solid sphere, *J. Fluid Mech.* **499**, 139 (2004).
 - [5] C. Duez, C. Ybert, C. Clanet, and L. Bocquet, Making a splash with water repellency, *Nat. Phys.* **3**, 180 (2007).
 - [6] L. Duck-Gyu and K. Ho-Young, Impact of a superhydrophobic sphere onto water, *Langmuir* **24**, 142 (2008).
 - [7] B. C. W. Tan, J. H. A. Vlaskamp, P. Denissenko, and P. J. Thomas, Cavity formation in the wake of falling spheres submerging into a stratified two-layer system of immiscible liquids, *J. Fluid Mech.* **790**, 33 (2016).
 - [8] S. Zhao, C. Wei, and W. Cong, Numerical investigation of water entry of half hydrophilic and half hydrophobic spheres, *Math. Probl. Eng.* **2016**, 5265818 (2016).

- [9] B. C. W. Tan and P. J. Thomas, Influence of an upper layer liquid on the phenomena and cavity formation associated with the entry of solid spheres into a stratified two-layer system of immiscible liquids, *Phys. Fluids* **30**, 064104 (2018).
- [10] D. Li, J. Zhang, M. Zhang, B. Huang, X. Ma, and G. Wang, Experimental study on water entry of spheres with different surface wettability, *Ocean Eng.* **187**, 106123 (2019).
- [11] D. L. Hu, B. Chan, and J. W. M. Bush, The hydrodynamics of water strider locomotion, *Nature (London)* **424**, 663 (2003).
- [12] J. W. M. Bush and D. L. Hu, Walking on water: Bioloocomotion at the interface, *Annu. Rev. Fluid Mech.* **38**, 339 (2006).
- [13] V. M. Ortega-Jimenez, L. von Rabenau, and R. Dudley, Escape jumping by three age classes of water striders from smooth, wavy and bubbling water surfaces, *J. Exp. Biol.* **220**, 2809 (2017).
- [14] J. M. Aristoff, T. T. Truscott, A. H. Techet, and J. W. M. Bush, The water entry cavity formed by low bond number impacts, *Phys. Fluids* **20**, 091111 (2008).
- [15] J. M. Aristoff and J. W. M. Bush, Water entry of small hydrophobic spheres, *J. Fluid Mech.* **619**, 45 (2009).
- [16] J. M. Aristoff, T. T. Truscott, A. H. Techet, and J. W. M. Bush, The water entry of decelerating spheres, *Phys. Fluids* **22**, 032102 (2010).
- [17] M. Do-Quang and G. Amberg, Numerical simulation of the coupling problems of a solid sphere impacting on a liquid free surface, *Math. Comput. Simul.* **80**, 1664 (2010), ESCO 2008 Conference.
- [18] T. T. Truscott and A. H. Techet, Water entry of spinning spheres, *J. Fluid Mech.* **625**, 135 (2009).
- [19] A. H. Techet and T. T. Truscott, Water entry of spinning hydrophobic and hydrophilic spheres, *J. Fluids Struct.* **27**, 716 (2011).
- [20] T. T. Truscott, B. P. Epps, and A. H. Techet, Unsteady forces on spheres during free-surface water entry, *J. Fluid Mech.* **704**, 173 (2012).
- [21] T. T. Truscott, B. P. Epps, and J. Belden, Water entry of projectiles, *Annu. Rev. Fluid Mech.* **46**, 355 (2013).
- [22] M. M. Mansoor, J. O. Marston, I. U. Vakarelski, and S. T. Thoroddsen, Water entry without surface seal: Extended cavity formation, *J. Fluid Mech.* **743**, 295 (2014).
- [23] D. Van Der Meer, Wrapping up a century of splashes, *J. Fluid Mech.* **800**, 1 (2016).
- [24] M.-H. Zhao, X.-P. Chen, and Q. Wang, Wetting failure of hydrophilic surfaces promoted by surface roughness, *Sci. Rep.* **4**, 5376 (2014).
- [25] I. U. Vakarelski, A. Jetly, and S. T. Thoroddsen, Stable-streamlined cavities following the impact of non-superhydrophobic spheres on water, *Soft Matter* **15**, 6278 (2019).
- [26] A. May, Effect of surface condition of a sphere on its water-entry cavity, *J. Appl. Phys.* **22**, 1219 (1951).
- [27] J. Shin and T. A. McMahon, The tuning of a splash, *Phys. Fluids A* **2**, 1312 (1990).
- [28] D. A. Watson, J. L. Stephen, and A. K. Dickerson, Jet amplification and cavity formation induced by penetrable fabrics in hydrophilic sphere entry, *Phys. Fluids* **30**, 082109 (2018).
- [29] D. A. Watson, J. L. Stephen, and A. K. Dickerson, Impacts of free-falling spheres onto a deep liquid pool with altered fluid and impactor surface conditions, *J. Vis. Exp.* **144**, e59300 (2019).
- [30] D. A. Watson, C. J. Souchik, M. P. Weinberg, J. M. Bom, and A. K. Dickerson, Making a splash with fabrics in hydrophilic sphere entry, *J. Fluids Struct.* **94**, 102907 (2020).
- [31] D. A. Watson, Interfacial properties modulate water entry dynamics for spherical projectiles, Doctoral Dissertation, College of Engineering and Computer Science, University of Central Florida, 2020.
- [32] See Supplemental Material at <http://link.aps.org/supplemental/10.1103/PhysRevFluids.6.044003> for eight movies and a supplementary document. The document contains descriptions of the movies, a close-up image showing flow separation around a $\beta = 90^\circ$ sphere, disaggregated plots with error bars to show the relation between nondimensionalized cavity depths κ/D and Fr for all water entry cases, position tracks for hemispherically coated spheres $\alpha = 0.33$, and $\alpha = 0.50$ with line of demarcation perpendicular to the free surface $\beta = 90^\circ$, and a supplementary figure showing lateral sphere migration induced by a thin, nonwoven fabric resting atop the liquid bath.

- [33] J. M. Cheny and K. Walters, Extravagant viscoelastic effects in the Worthington jet experiment, *J. Non-Newtonian Fluid Mech.* **67**, 125 (1996), Papers Presented at the Workshop on Unresolved Experimental Dilemmas in the Dynamics of Complex Fluids.
- [34] A. Ogawa, K. Utsuno, M. Mutou, S. Kouzen, Y. Shimotake, and Y. Satou, Morphological study of cavity and Worthington jet formations for Newtonian and non-Newtonian liquids, *Part. Sci. Technol.* **24**, 181 (2006).
- [35] S. Gekle, J. M. Gordillo, D. van der Meer, and D. Lohse, High-Speed Jet Formation After Solid Object Impact, *Phys. Rev. Lett.* **102**, 034502 (2009).
- [36] J. M. Gordillo and S. Gekle, Generation and breakup of worthington jets after cavity collapse. part 2. tip breakup of stretched jets, *J. Fluid Mech.* **663**, 331 (2010).
- [37] S. Gekle and J. M. Gordillo, Generation and breakup of Worthington jets after cavity collapse. Part 1. Jet formation, *J. Fluid Mech.* **663**, 293 (2010).
- [38] G. E. Cossali, M. Marengo, A. Coghe, and S. Zhdanov, The role of time in single drop splash on thin film, *Exp. Fluids* **36**, 888 (2004).
- [39] N. B. Speirs, M. M. Mansoor, J. Belden, and T. T. Truscott, Water entry of spheres with various contact angles, *J. Fluid Mech.* **862**, R3 (2019).
- [40] K. G. Bodily, S. J. Carlson, and T. T. Truscott, The water entry of slender axisymmetric bodies, *Phys. Fluids* **26**, 072108 (2014).
- [41] N. B. Speirs, Z. Pan, J. Belden, and T. T. Truscott, The water entry of multidroplet streams and jets, *J. Fluid Mech.* **844**, 1084 (2018).
- [42] Y. Ueda and M. Iguchi, Water entry of stripe-coated hydrophobic circular cylinders, *J. Visualization* **15**, 33 (2012).
- [43] D. Gilbarg and R. A. Anderson, Influence of atmospheric pressure on the phenomena accompanying the entry of spheres into water, *J. Appl. Phys.* **19**, 127 (1948).
- [44] J. O. Marston, T. T. Truscott, N. B. Speirs, M. M. Mansoor, and S. T. Thoroddsen, Crown sealing and buckling instability during water entry of spheres, *J. Fluid Mech.* **794**, 506 (2016).
- [45] M. Beczek, M. Ryzak, A. Sochan, R. Mazur, C. Polakowski, and A. Bieganski, The differences in crown formation during the splash on the thin water layers formed on the saturated soil surface and model surface, *PLoS ONE* **12**, e0181974 (2017).
- [46] M. E. Alam, D. Wu, and A. K. Dickerson, Predictive modeling of drop ejection from damped, dampened wings by machine learning, *Proc. R. Soc. London Ser. A* **476**, 20200467 (2020).
- [47] E. Castillo-Orozco, A. Davanlou, P. K. Choudhury, and R. Kumar, Droplet impact on deep liquid pools: Rayleigh jet to formation of secondary droplets, *Phys. Rev. E* **92**, 053022 (2015).
- [48] S. R. Krishnan and C. S. Seelamantula, On the selection of optimum Savitzky-Golay filters, *IEEE Trans. Signal Process.* **61**, 380 (2013).
- [49] W. Peters and J. Spurgeon, Biology of the water-boatman *Krizousacorixa femorata* (heteroptera: Corixidae), *Am. Midl. Nat.* **86**, 197 (1971).
- [50] R. W. Blake, Hydrodynamics of swimming in the water boatman, *Cenocorixa bifida*, *Can. J. Zool.* **64**, 1606 (1986).
- [51] V. Ngo and M. J. McHenry, The hydrodynamics of swimming at intermediate Reynolds numbers in the water boatman (corixidae), *J. Exp. Biol.* **217**, 2740 (2014).
- [52] D. R. Jones, Factors affecting the recovery from diving bradycardia in the frog, *J. Exp. Biol.* **44**, 397 (1966).
- [53] N. H. West and D. R. Jones, The initiation of diving apnoea in the frog, *Rana pipiens*, *J. Exp. Biol.* **64**, 25 (1976).
- [54] Y. Kubota, O. Mochizuki *et al.*, Splash formation due to a frog diving into water, *World J. Mech.* **5**, 129 (2015).
- [55] O. T. Owre, Adaptations for Locomotion and Feeding in the Anhinga and the Double-crested Cormorant, *Ornithological Monographs* **6**, 1 (1967).

- [56] K. Hustler, Buoyancy and its constraints on the underwater foraging behavior of reed cormorants *Phalacrocorax africanus* and darters *Anhinga melanogaster*, [Ibis](#) **134**, 229 (1992).
- [57] P. G. Ryan, Diving in shallow water: The foraging ecology of darters (aves: Anhingidae), [J. Avian Biol.](#) **38**, 507 (2007).
- [58] N. B. Speirs, M. M. Mansoor, R. C. Hurd, S. I. Sharker, W. G. Robinson, B. J. Williams, and T. T. Truscott, Entry of a sphere into a water-surfactant mixture and the effect of a bubble layer, [Phys. Rev. Fluids](#) **3**, 104004 (2018).